polymers

MDPI

Article

Py–FTIR–GC/MS Analysis of Volatile Products of Automobile Shredder Residue Pyrolysis

Bin Yang and Ming Chen *

School of Mechanical Engineering, Shanghai Jiao Tong University, No. 800, Dongchuan Rd., Shanghai 200240, China; robinshjt@sjtu.edu.cn

* Correspondence: mingchen@sjtu.edu.cn

Received: 15 October 2020; Accepted: 17 November 2020; Published: 18 November 2020

Abstract: Automobile shredder residue (ASR) pyrolysis produces solid, liquid, and gaseous products, particularly pyrolysis oil and gas, which could be used as renewable alternative energy resources. Due to the primary pyrolysis reaction not being complete, the yield of gaseous product is low. The pyrolysis tar comprises chemically unstable volatiles before condensing into liquid. Understanding the characteristics of volatile products will aid the design and improvement of subsequent processes. In order to accurately analyze the chemical characteristics and yields of volatile products of ASR primary pyrolysis, TG–FTIR–GC/MS analysis technology was used. According to the analysis results of the Gram–Schmidt profiles, the 3D stack plots, and GC/MS chromatograms of MixASR, ASR, and its main components, the major pyrolytic products of ASR included alkanes, olefins, and alcohols, and both had dense and indistinguishable weak peaks in the wavenumber range of 1900–1400 cm^{-1}. Many of these products have unstable or weaker chemical bonds, such as =CH–, =CH2, –C=C–, and –C=CH2. Hence, more syngas with higher heating values can be obtained with further catalytic pyrolysis gasification, steam gasification, or higher temperature pyrolysis.

Keywords: automobile shredder residue (ASR); pyrolysis; thermogravimetric analysis; gas chromatograph; gas chromatography mass spectrometry; Fourier transform infrared spectrometry

1. Introduction

The dismantling and recycling of end-of-life vehicles (ELVs) is not only an important way to save resources and realize sustainable development but also bears huge social and environmental responsibility. As of the end of 2019, China's car ownership exceeded 260 million. According to the international scrap ratio of 4–6%, the quantity of ELVs in China will be large in the future. Automobile shredder residue (ASR) accounts for about 20–25% of a vehicle's weight [1–6] and consists of plastic, textile, leather, rubber, foam, wood, paper, glass, sand, metals, and other materials [3–8]. Organic components account for about 60–85% of ASR [9,10], for which thermal conversion technology represents a viable resource recovery process. Pyrolysis and gasification have gradually become the main means to dispose of ASR, since they can reduce the volume and quality of landfill with lower cost, while energy recovery can be carried out simultaneously [11–13]. ASR pyrolysis produces solid, liquid, and gaseous products, particularly pyrolysis oil and gas, which could be used as renewable alternative energy resources.

The yields and characteristics of ASR pyrolytic products depend on the feed (e.g., fractions of organic versus inorganic), temperature, residence time, and carrier gases used [12]. There is a great range of variations possible, and the values used in a given process design must be chosen depending on which products are the process targets. Harder and Forton analyzed the variations in the physical characteristics of ASR, provided a review of the current technical developments in pyrolysis processes, and emphasized that the energy content of ASR is crucial to the design of a thermal process [14].

Zolezzi et al. evaluated the performance and product yields of conversional and fast pyrolysis of ASR at different temperatures [12]. It proved that the gas yield in conventional pyrolysis was higher than in fast pyrolysis, and higher heating values (HHVs) of gas increased with increasing temperature. HHV gas is also the optimal pyrolytic product of our research project funded by the National Natural Science Foundation of China No. 51675343. Extensive experimental research into ASR pyrolysis by other authors [15–20] has shown CO, CO_2, H_2, and light hydrocarbons (C1–C4, such as CH_4, C_2H_2, C_2H_4, C_2H_6, C_3H_6) as the dominant constituents of HHV gas. We also studied the pyrolytic product yields and characterizations of gaseous products (H_2, CO, CO_2, CH_4, C_2H_4, C_2H_6, C_3H_6 and C_3H_8), which were analyzed in laboratory-scale non-isothermal pyrolysis experiments at finished temperatures of 500, 600, and 700 °C [21]. Moreover, we found that the pyrolytic reaction was insufficient in primary ASR pyrolysis, and the yield and calorific value of HHV gas are limited. Since the yield of gaseous product is low, however, the yield of tar and char are always higher. Our previous results show that tar and gas accounted for 39.68 and 19.76% of the pyrolysis product when the pyrolysis temperature was set to 600 °C [21].

Catalytic pyrolysis gasification [22–24], steam gasification [25,26], and higher temperature pyrolysis [27] are effective methods of increasing HHV gas production. Aiming to improve the yields of syngas and hydrogen, a two-stage pyrolysis process with catalysts was designed in our research project. Before the polymer organic mixtures pyrolyzed in the first-stage reactor condensed into tar, secondary pyrolysis was expected to continue under the action of catalysts. Lin et al. [28] presented an analysis of the catalytic gasification of ASR for the generation of high-purity hydrogen in a lab-scale fixed-bed downdraft gasifier using 15 wt.% NiO/Al_2O_3 catalysts at 760–900 K. They verified that the NiO/Al_2O_3 catalysts can increase the output of hydrogen and CO, but did not explain how the catalyst affects the secondary reaction of pyrolysis intermediate products. The main challenges of implementing and improving catalytic gasification technology were to select or develop suitable catalysts for enhancing synthesis gas yield. Most pyrolysis tar is also volatile before condensing into liquid, and its chemical state is very unstable. Understanding the characteristics of volatile products will aid the design and improvement of subsequent processes. Thus, the purpose of this study was to analyze the chemical compositions and yields of volatile products of primary ASR pyrolysis.

Thermogravimetric analysis (TGA), coupled with Fourier transform infrared spectrometry (FTIR) and gas chromatography–mass spectrometry (GC/MS), is a good means by which to explore not only the weight loss characteristics and kinetics parameters of the thermal pyrolysis process but also identify the gaseous byproduct generated in real time. Kai et al. [29] investigated the effects of the interaction between rice straw (RS) and high-density polyethylene (HDPE) on the evolution of volatile species and their distributions during the co-pyrolysis of RS and HDPE by TG–FTIR–MS. Wu et al. [30] analyzed the pyrolysis and co-pyrolysis behaviors of polyethylene (PE), polystyrene (PS), and polyvinyl chloride (PVC) under N_2 atmosphere by TG–FTIR. Zhang et al. [31] investigated the thermal decomposition of six representative components of municipal solid waste (MSW, including lignin, printing paper, cotton, rubber, PVC, and cabbage). Surjit Singh et al. [32] reported the characterization and assessment of the volatile species evolved during the thermal degradation of several waste materials, biomass wood waste, refuse derived fuel (RDF), waste plastic, and tire by use of TGA–FTIR and TGA–MS. Guo et al. [33] analyzed gas emissions from the thermo-oxidative process of plastic ASR under different N_2/O_2 volume ratios using TG–MS analysis, but only the production changes of small molecular gases under different reaction conditions were considered, such as H_2, CH_4, NH_3, HCN, NO, NO_2, CO_2, and SO_2. Mayyas et al. [34] studied the effect of the TiO_2 catalyst on the pyrolyzed byproducts of industrial plastic waste (i.e., automotive shredder residue, ASR) with TG–FTIR–GC/MS. In our study, in the TGA experiments for ASR, each main component (plastic, textile, leather, rubber, foam) and artificial mixture was examined with a thermogravimetric analyzer under non-isothermal conditions. Simultaneously, the chemical compositions of volatile products of the primary ASR pyrolysis and its main components were detected and identified by TG–FTIR–GC/MS.

2. Experimental Procedure and Specimens

2.1. Experimental Specimens

The ASR specimens studied in this work were obtained from the Zhangjiagang Huaren Resources Recycling Co., Ltd. (Zhangjiagang, Jiangsu Province, China), a domestic automobile dismantling enterprise. Reusable components with market value and particularly valuable material fractions such as batteries, air bags, tires, and catalytic converters are usually removed from ELVs. The remaining parts and the hulks are reduced to small pieces, most of the metal fraction is sorted using magnetic separation and eddy current separation, and the remaining fraction is called ASR, which amounts to ~20–25% of the average input ELV weight. ASR initial specimens were continuously obtained over one week from a crushing and sorting production line for ELVs. Visible bulks of metal to the human eye were sought out from the ASR initial specimens. The characteristics of the ASR specimens were determined by manual sorting and with a Mettler Toledo analytical balance (Changzhou, Jiangsu Province, China), and the results are shown in Table 1.

Table 1. Material compositions of the experimental specimens.

Sample	Material Composition (wt.%)						
	Metals	Plastics	Textiles	Leather	Rubber	Foam	Others
ASR	3.0	39.7	28.1	3.3	2.2	2.1	21.6
MixASR	0	53	37	3	4	3	0

All specimens were combined and mixed well to ensure a representative sample for the determination, and the uniformity of all specimens regarding the particle size (approximately ≤0.1 mm) was achieved. The reaction mechanism of ASR was unknown, so keeping the initial mass of each sample at a fixed constant for all measurements was safe [35]. Thus, the mass of all samples for the TG experiments was 100 ± 0.1 mg, considering the size of the sample pan and the accuracy of balance in the thermogravimetric analyzer.

2.2. Experimental Procedure

The TG–FTIR–GC/MS coupling technique is widely used in the analysis of organic pyrolysis behaviors. Therefore, we studied the pyrosis behaviors of ASR and its five main components with the TG–FTIR–GC/MS coupling technique. As shown in Figure 1, GC/MS (Perkin-Elmer SQ 8, Waltham, MA, USA) and FTIR (Perkin-Elmer TL 9000, Waltham, MA, USA) equipment was connected with a TG analyzer (Perkin-Elmer TGA 8000, Waltham, MA, USA), and all transmission lines were heated and maintained at 270 °C to prevent the condensation of any volatile disintegration products. Pyris-Manager software was used to analyze the TG and derivate TG (DTG) data, TimeBase Version 3.1.0 (Perkin-Elmer, Waltham, MA, USA) and Spectrum Version 10.5.3 (Perkin-Elmer, Waltham, MA, USA) were applied for the analysis of FTIR spectra data, and the mass spectra data were analyzed using TurboMass Ver 6.0.0 (Perkin-Elmer, Waltham, MA, USA).

The reaction evolution of plastic, textiles, rubber, leather, foam, ASR, and MixASR was recorded for a full range of temperatures from 30 to 800 °C at a constant heating rate of 10 °C/min under atmospheric control with high-purity (99.99%) nitrogen at a rate of 20.0 mL/min. The pressures of pneumatic gas and balance gas were set to 0.1 and 0.2 MPa, respectively. This nitrogen flow rate ensures an inert atmosphere for the sample during the run, whereas a small sample and slow heating rate ensures that the heat transfer limitations can be ignored. Gaseous products from the TG analyzer were directly collected in the gas cell and determined instantaneously using the Fourier transform infrared spectrometer. The resolution in FTIR was 4 cm^{-1}, and the scan range was from 4000 to 450 cm^{-1}. The FTIR spectra of the gaseous products were obtained continuously with the baseline modified. After the FTIR measurements, the gas products were instantaneously swept to the mass spectrometer.

The oven temperature was heated and maintained at 270 °C, and the ionization energy under the electron-impact (EI) of gas volatiles was analyzed at 70 eV. The mass-to-ion ratio (*m*/*z*) ranged from 45 to 400 and was scanned 200 times per minute.

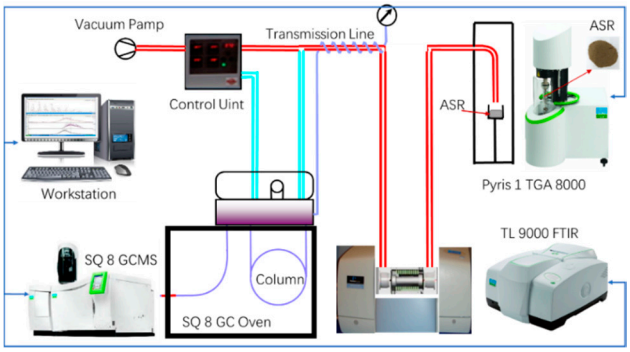

Figure 1. Layout diagram of TG–FTIR–GC–MS (provided by PerkinElmer, MA, USA).

3. Results and Discussion

3.1. FTIR Analysis of Volatile Products

FTIR is an effective analytical instrument for detecting functional groups and characterizing covalent bonding information. In this study, the Fourier transform infrared spectra of pyrolytic product of plastic, textile, rubber, leather, foam, ASR, and MixASR were recorded to certify the basic chemical group of thermal decomposition product. As shown in Figure 2, Gram–Schmidt profiles of plastic, textile, MixASR, and ASR had only one significant peak, while the Gram–Schmidt profiles of rubber, leather, and foam had two peaks. Below 300 °C, the pyrolysis reactions of ASR, MixASR, or its main components were slow or nonexistent. Over 300 °C, the pyrolysis reactions of rubber, leather, and foam were rapid; the first peak appeared at 346, 322, and 371 °C, respectively, while the second peak appeared at 536, 533, and 452 °C, respectively. Pyrolysis reactions of plastic and textile mainly occurred in the temperature range of 400 to 600 °C, and the only peak appeared at 525 and 515 °C, respectively. Reaching 620 °C, the pyrolysis reaction of plastic, rubber, leather, textile and foam was basically completed, and the curve dropped sharply. The pyrolysis reaction of MixASR mainly occurred in the range of 400–600 °C, and the peak temperature was 526 °C. In addition to the five major organic components, ASR contains 24.6% of other substances in this study, so Gram–Schmidt profiles of ASR and MixASR were very different, but peaks both appeared at 526 °C. The reason is that plastics and fibers accounted for a high proportion of ASR and MixASR, which were the main substances affecting pyrolytic products.

According to the 3D stack plots of MixASR and ASR in Figure 3, the wavenumber ranges of absorption peaks are different. The main absorption peaks in the 3D stack plots of plastic and textiles also appear in the same wavenumber ranges in the 3D stack plots of ASR and MixASR. However, the intensity of the absorption peak at a certain position of MixASR or ASR is not the linear superposition result of the intensities of the absorption peaks at the same position of the five components. In short, the pyrolysis product of ASR is not a simple superposition of the pyrolysis products of its components, but the pyrolysis characteristics of the main components have the greatest influence on the product distribution, especially plastic and textiles.

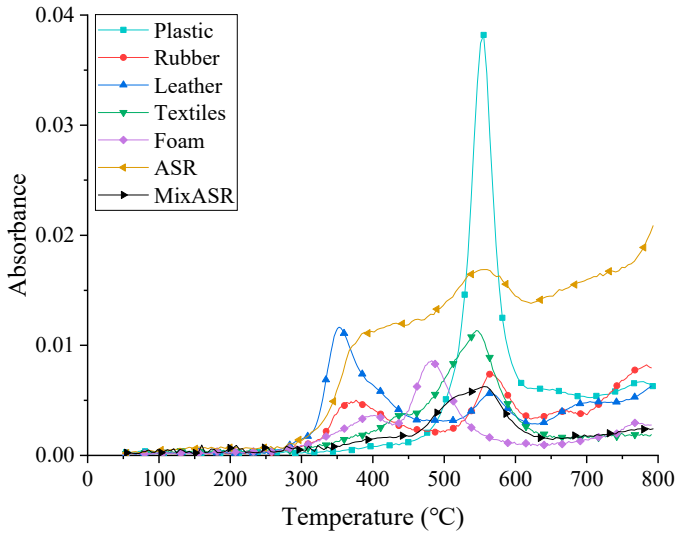

Figure 2. Gram–Schmidt profiles of automobile shredder residue (ASR), MixASR, and its main components.

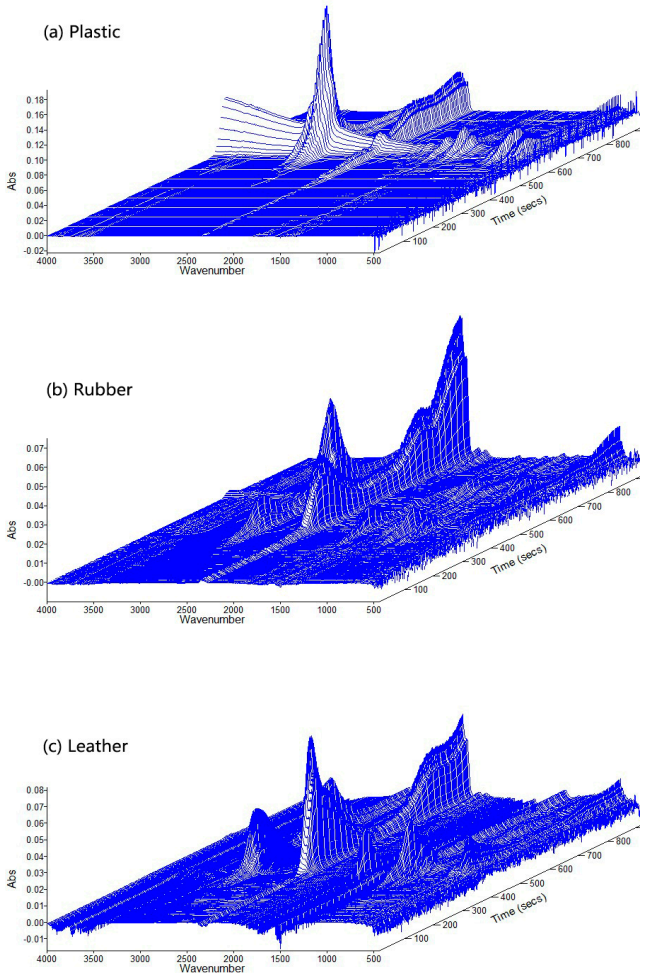

Figure 3. *Cont.*

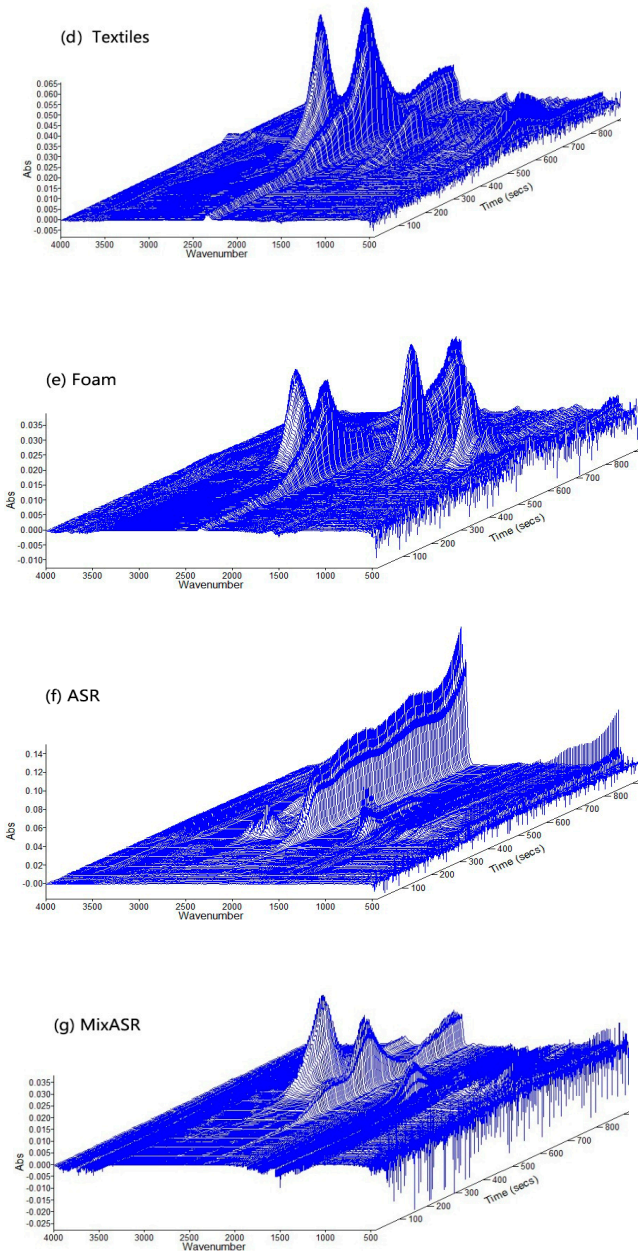

Figure 3. The 3D stack plots of MixASR, ASR, and its main components.

With TimeBase and Spectrum software (Perkin-Elmer, Waltham, MA, USA), the Gram–Schmidt profiles of samples were analyzed, and the FTIR spectra of ASR, MixASR, its main components at 200, 300, 400, 500, 600, 700 °C, and temperatures of peaks of Gram–Schmidt profiles are shown in Figures 4 and 5. These functional groups are useful for distinguishing some specific chemical compounds, like CO_2, alkanes, olefins, benzene, alcohols, and other organic components. According to Figures 4a–e and 5, it can be observed that the locations of the absorption bands were almost the same for the same sample, but the absorbance intensities were different After pyrolysis, the temperature was higher than 300 °C. This indicated that the major categories of volatile products were not affected by the pyrolysis temperature, but the yield of each main product was still affected by the pyrolysis temperature. Strong absorption peaks appeared at 3100–2700, 1700–1550, and 1500–1250 cm^{-1} for ASR and its main components, which were assigned to the stretching of $=CH_2$, $–CH_3$, $–CH_2$, –CH–, and C=C bonds. Furthermore, the absorption intensity of the corresponding macromolecules such as alkanes, aldehydes, and alcohols increased with pyrolysis temperatures and increased sharply at the

peak temperatures of the Gram–Schmidt profiles, then sharply decreased. The bands of stretching of =CH–, stretching of –C=C–, and plane –CH– bending –C=CH_2 were assigned to the alkenes. The strong absorption peaks of 2930, 2850, and 1460 cm^{-1} certify the existence of the methylene (–CH_2–) group. The formation mechanisms of–CH– and C=C bonds were cleavage of alkyl side chains and β bond scission of alkenes. CO_2 is represented by the peak between 2395 and 2250 cm^{-1} for ASR and its main components, and the production of CO_2 increased with temperature, peaked at the first pyrolysis peak temperature, and then decreased sharply. After exceeding 500 °C, peaks appeared between 720–570 and 1050–1150 cm^{-1}, which were assigned to the symmetric stretching of C–O. Meanwhile, the CO at 2109–2173 cm^{-1} can also be detected in the entire pyrolysis process. In addition to these substances, each component of ASR had relatively independent functional groups, but which eventually appeared in the mixture FTIR spectrum.

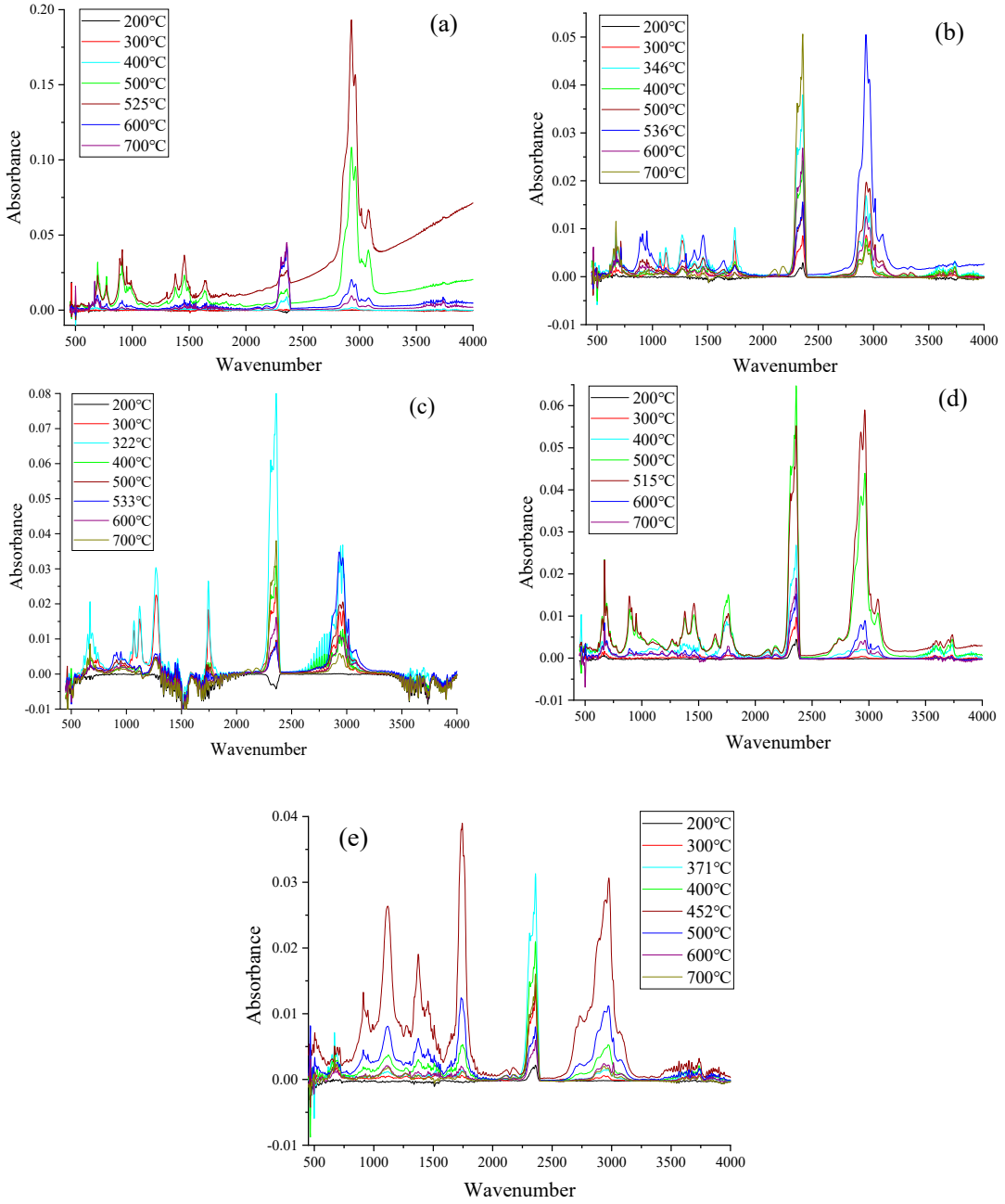

Figure 4. The FTIR spectrum of components of ASR at different pyrolysis temperatures: (**a**) plastic; (**b**) rubber; (**c**) leather; (**d**) textile; and (**e**) foam.

For plastic, the major pyrolytic products were alkanes and olefins, such as styrene, 3-ethyl-3-methyl heptane, and 2,4-dimethyl-1heptene, since the bonds of stretching =CH2, $–CH_3$, $–CH_2$, –CH– and bending $RHC=CH_2$ were assigned. The major pyrolytic products of textiles were CO_2, alkanes, olefins, benzene, and alcohols, e.g., 2,6-dimethylnonane, styrene, and 2-methyl-1-pentene. Except for CO_2, alkanes, olefins, and benzene series, the major pyrolytic products of rubber and leather also included alcohols, since the bands of stretching of alcoholic C–OH were assigned to the alcohols, e.g., 1-phenyl-2-propanol. The major pyrolytic products of foam were different; ketones were identified by the bonds of stretching keto C=O, e.g., 1-isopropoxy-propan-2-one. Compared with other components, there are more alkanes and alcohols in foam pyrolysis products.

The major pyrolytic products of ASR and MixASR were much the same, which included alkanes, olefins, and alcohols, and both had dense and indistinguishable weak peaks in the wavenumber range of 1900–1400 cm^{-1}. Obviously, many of these products have unstable or weaker chemical bonds, which can be further pyrolyzed under further high-temperature (>800 °C) or catalytic pyrolysis.

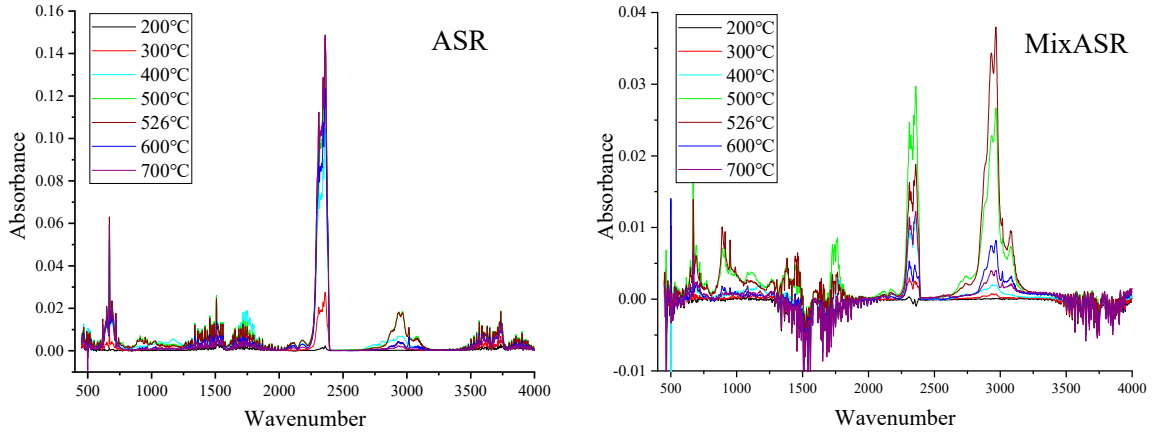

Figure 5. The FTIR spectrum of ASR and MixASR at different pyrolysis temperatures.

3.2. GC/MS Analysis of Volatile Products of ASR Pyrolysis

In the accurate identification of complicated volatile species, MS analysis is a useful complementary technique for TG–FTIR because TG–FTIR cannot measure homodiatomic species. In order to further accurately analyze the compound types and yields of volatile products of ASR pyrolysis, GC–MS analysis technology was used. The detectable compound was that with a concentration above the detection limit of GC–MS, while the identifiable compound by the NIST library was that with a comparatively large peak area. Since there is no distinguishable peak after 15 min, the chromatogram for the range from 0 to 15 min is shown in Figure 6. Moreover, during the identification of chemical compounds of volatile products, the radicals and functional groups evolved at peaks were based on the results of FTIR analysis. The identification results including compound names and yields of volatile pyrolytic products of ASR and its main components were summarized and are provided in Tables 2 and 3, and Appendix A. According to the GC–MS analysis results, several points were concluded as follows:

(1) The identified gaseous pyrolytic products were both composed of alkanes, olefins, alcohols, and benzene series, which were consistent with the analysis results of FTIR. The gaseous pyrolytic products of MixASR and ASR were not the simple superposition of pyrolytic gaseous products of its components, but main compounds of MixASR and ASR also appeared in the pyrolytic products of its main components, especially plastic and textile, e.g., styrene, 1-hexene, toluene, ethylbenzene, 2,4-dimethyl-1heptene, and 11-methyl-1-dodecanol.

(2) In the volatile products of the plastics, rubber, leather, textiles, and foam pyrolysis, the total proportions of detectable macromolecular substances were 26.2634, 34.9797, 39.0640, 54.1273, and 39.2296%, respectively. The pyrolysis product of plastic contains 6.0263% olefins, 2.5443%

alcohols, 15.25114% benzene series, and very few alkanes. The pyrolysis product of the rubber component contains 13.3232% alkanes, 4.7653% olefins, and 4.6502% alcohols. The leather component pyrolysis product contains 3.3224% alkanes, 7.1102% alkenes, 6.4884% alcohols, and 7.4626% ethers. The pyrolysis products of textiles components contained 1.1139% alkanes, 20.4953% olefins, 7.5055% alcohols, and 15.9611% benzene series. The pyrolysis products of foam components contained 6.8049% alkanes, 12.4046% olefins, 2.4621% ethers, 1.8138% benzene series, and 13.4151% ketones.

(3) The total proportions of detectable macromolecular substances in the volatile products of the original ASR and MixASR pyrolysis were 41.884% and 40.2709%, respectively. The specific detected substances are shown in Tables 2 and 3. The ASR pyrolysis product contains 3.7385% alkanes, 26.5539% alkenes, and 9.3305% benzene series. The MixASR pyrolysis products contains 0.4045% alkanes, 2.1909% olefins, and 17.739% benzene series. From the comparison of the yield of various pyrolysis products, it can also be seen that the pyrolysis products of ASR or MixASR are not the linear superposition of the pyrolysis products of its main components. This shows once again that the main components of ASR have obvious interactions in the pyrolysis process, and this effect affects the product distribution.

(4) Based on the GC–MS analysis results of ASR and its main components, it can be seen that the yields of olefin and benzene series are high in the pyrolytic products, especially styrene. In pyrolytic products of plastic, textiles, foam, ASR, and MixASR, styrene accounted for 13.62, 11.64, 11.93, 17.18, and 20.68%, respectively. However, these substances are chemically unstable and can be further reacted by improving the process to generate more CO and H_2.

Table 2. GC–MS analysis results of the original ASR pyrolysis volatiles.

No.	Peaks	Formula	Compound	CAS Number	Yield/%
1	2.226	$C_8H_{16}O$	1-prop-2-enoxypentane	23186-70-1	2.8681
2	2.445	C_3H_9NO	1-aminopropan-2-ol	78-96-6	0.4912
3	2.544	C_6H_{12}	1-hexene	592-41-6	0.8056
		C_6H_{12}	4-methyl-1-Pentene	691-37-2	
		$C_6H_{13}Cl$	2-chlorohexane	638-28-8	
4	2.771	C_4H_8O	tetrahydrofuran	109-99-9	0.2440
		$C_5H_{10}O_2$	4-ethyl-1,3-dioxolane	29921-38-8	
5	3.037	$C_6H_{11}ClO$	α-chlorohexanal	762-39-0	2.6292
6	3.508	$C_7H_{12}O_3$	2-methylacrylic acid 3-hydroxypropyl ester	2761-09-3	0.8626
		$C_7H_{12}O_3$	2-hydroxypropyl methacrylate	923-26-2	
7	4.364	C_7H_8	toluene	108-88-3	4.1164
8	4.798	$C_8H_{18}O$	2,3-dimethylhexan-3-ol	4166-46-5	0.2205
		$C_6H_{14}O$	4-Methyl-2-pentanol	108-11-2	
9	5.147	$C_6H_{12}O_2$	1-isopropoxy-propan-2-one	42781-12-4	0.3793
10	5.623	C_9H_{18}	2,4-dimethyl-1heptene	19549-87-2	1.6540
11	6.026	C_8H_{10}	ethylbenzene	100-41-4	1.2742
			o-Xylene	95-47-6	
12	6.593	C_8H_8	annulene	629-20-9	20.6849
			benzocyclobutene	694-87-1	
			styrene	100-42-5	
13	7.205	C_9H_{12}	cumene	98-82-8	0.0749
14	7.614	C_9H_{10}	prop-2-enylbenzene	300-57-2	0.1990
15	8.127	C_6H_6O	phenol	108-95-2	0.3113
16	8.181	$C_8H_{14}O_2$	butyl methacrylate	97-88-1	0.2616
17	8.274	C_9H_{10}	2-phenyl-1-propene	98-83-9	3.0575

Table 2. *Cont.*

No.	Peaks	Formula	Compound	CAS Number	Yield/%
18	8.717	$C_{14}H_{30}$ $C_{10}H_{22}$	7-methyltridecane 3-ethyl-3-methyl heptane	26730-14-3 17302-01-1	0.0597
19	9.06	$C_8H_{18}O$	2-ethylhexan-1-ol 2-propylpentan-1-ol	104-76-7 58175-57-8	0.8311
20	9.142	C_8H_{16}	3,4,4-trimethyl-2-pentene 2,4,4-trimethyl-2-pentene	598-96-9 107-40-4	0.2199
21	9.36	$C_{10}H_{12}$	4-phenyl-1-butene	768-56-9	0.1319
22	9.601	$C_{10}H_{12}$	alpha,p-dimethylstyrene	1195-32-0	0.2256
23	9.754	C_8H_8O	acetophenone	98-86-2	0.0718
24	9.907	$C_{13}H_{28}O$	11-methyl-1-dodecanol	85763-57-1	0.2098

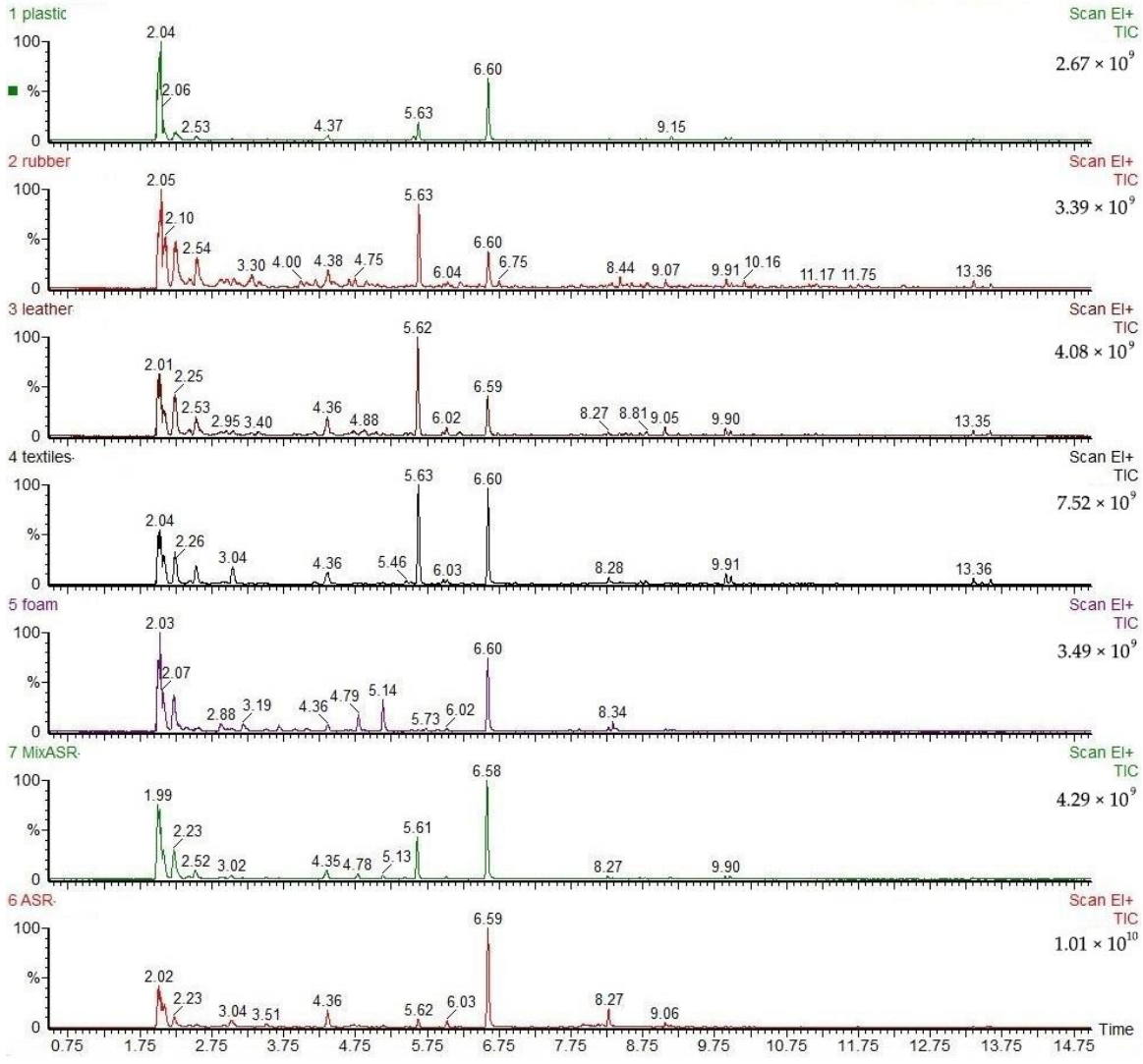

Figure 6. The total ions chromatogram (TIC) of samples at representative temperatures.

3.3. Analysis, Summary, and Discussion

According to the Py–FTIR–GC–MS analysis, the pyrolysis process of ASR could be concluded as follows. Firstly, small molecule alkenes and cycloalkenes were generated from the degradation of ASR due to chain scission at low temperature. Then, the released alkenes and cycloalkenes underwent a series of reactions to form benzene and benzene derivatives as the pyrolysis temperature increased.

The main pyrolysis products were concentrated in alkenes, olefins, alcohols, and aromatic hydrocarbons. The yields of volatile products of ASR pyrolysis varied greatly with changing pyrolysis temperature. Considering that plastic and textiles account for a high proportion of ASR, and other organic matter is affected by them during the pyrolysis process [21], the design of pyrolysis temperature can refer to the pyrolysis characteristics of plastics and fibers. Since most volatile products are chemically unstable, more syngas with a greater calorific value could be obtained by catalytic pyrolysis and gasification [36–38].

Table 3. GC–MS analysis results of the MixASR pyrolysis volatiles.

No.	Peaks	Formula	Compound	CAS Number	Yield/%
1	2.229	$C_6H_{12}O$	1-prop-2-enoxypropane	1471-03-0	8.1671
2	2.431	$C_7H_{10}O_6$	methanetricarboxylic acid, 1,1,1-trimethyl ester	1186-73-8	0.4723
3	2.521	C_6H_{12}	2-methyl-1-pentene 1-hexene	763-29-1 592-41-6	1.9019
4	4.347	$C_9H_{12}O$	1-phenyl-2-propanol	698-87-3	2.0945
5	4.784	$C_6H_{14}O$	4-methyl-2-pentanol	108-11-2	0.8483
6	5.13	$C_6H_{12}O_2$	1-isopropoxy-propan-2-one	42781-12-4	0.7124
7	5.609	C_9H_{18}	2,4-dimethyl-1heptene	19549-87-2	6.9013
8	6.0009	C_8H_{10}	ethylbenzene o-xylene	100-41-4 95-47-6	0.2366
9	6.579	C_8H_8	styrene	100-42-5	17.1758
10	8.266	C_9H_{10}	2-phenyl-1-propene	98-83-9	0.3269
11	8.702	$C_{10}H_{22}$ $C_{11}H_{24}$ $C_{14}H_{30}$	3-ethyl-3-methyl heptane 2,6-dimethylnonane dodecane,4,6-dimethyl	17302-01-1 17302-28-2 61141-72-8	0.4045
12	9.136	$C_{10}H_{16}$	(3R)-(+)-isosylvestren	1461-27-4	0.2890
13	9.902	$C_{13}H_{28}O$	11-methyl-1-dodecanol	85763-57-1	0.7403

4. Conclusions

In this work, efforts were made to investigate the pyrolysis characteristics of ASR and its main components (i.e., plastic, textile, leather, rubber, and foam) through TG–FTIR-GC–MS. The mass variation of samples and the gaseous products were measured simultaneously. Comparing the results of FTIR and GC–MS analysis, good consistency between these two approaches was observed, and the main conclusions can be summarized as follows:

(1) The main volatile products of ASR and its main components are alkanes, olefins, alcohols, and benzene series, and their proportions in the pyrolysis products are 3.7385, 26.5539, and 9.3305%, respectively. Many of these volatile products have unstable or weaker chemical bonds, such as =CH–, $=CH_2$, –C=C–, and $–C=CH_2$. Hence, more syngas can be obtained with further high-temperature (>800 °C) pyrolysis [39,40]. Catalytic pyrolysis and gasification are important research directions for obtaining syngas with a greater calorific value [36–38].

(2) According to the Gram–Schmidt profiles and the 3D stack plots of MixASR, ASR, and its main components, the pyrolysis product of ASR is not a simple superposition of the pyrolysis products of its components, but the pyrolysis characteristics of the main components have the greatest influence on the product distribution, especially plastic and textiles. Some hazardous gas exists in pyrolytic products of ASR, such as benzene and toluene, which are harmful to the human body and environment. Therefore, the elimination of toxic and hazardous substances must be considered in the design of pyrolysis process.

In brief, the TG–FTIR–GC–MS coupling technique provided a deeper insight into the understanding of pyrolysis behaviors of ASR. This is helpful for the design of further pyrolysis processes for obtaining more syngas with higher heating value. It could also provide basic information for an industrial pilot or industrialization of the ASR or polymer pyrolysis process.

Author Contributions: Conceptualization, methodology, investigation and resources: B.Y. and M.C.; software, validation, formal analysis, data curation, writing—original draft preparation, writing—review and editing, visualization: B.Y.; supervision, project administration and funding acquisition: M.C. All authors have read and agreed to the published version of the manuscript.

Funding: This research was funded by the National Natural Science Foundation of China No.51675343. http://www.nsfc.gov.cn/. Responsibility for the information and views set out in this article lies entirely with the authors.

Acknowledgments: The authors express their sincerest thanks to the National Natural Science Foundation of China for financing this research within the program "Fundamental Research on Catalytic Gasification of Automobile Shredder Residues (ASR): Mechanism and Its Recovery" under grant number 51675343.

Conflicts of Interest: The authors declare no conflict of interest.

Abbreviations

The following abbreviations are used in this manuscript:

ASR	Automobile shredder residue
MixASR	Mixtures of plastic, textiles, leather, rubber, and foam
Py	Pyrolysis
FTIR	Fourier transform infrared spectrometry
GC/MS	Gas chromatography–mass spectrometry
PVC	Polyvinyl chloride
TGA	Thermogravimetry analysis
HHVs	Higher heating values

Appendix A

Table A1. GC–MS analysis results of the plastic pyrolysis volatiles.

No.	Peaks	Formula	Compound	CAS Number	Yield/%
1	2.249	$C_6H_{10}O$	6-methyl-3,6-dihydro-2H-pyran	55230-25-6	3.5802
2	2.533	C_6H_{12}	2-methyl-1-pentene	763-29-1	1.0352
3	3.517	$C_5H_8O_2$	methyl methacrylate	80-62-6	0.1645
3	4.37	$C_9H_{12}O$	1-phenyl-2-propanol	698-87-3	1.5010
5	5.558	C_8H_{12}	4-vinyl-1-cyclohexene	100-40-3	0.5372
		C_9H_{18}	2,4-dimethyl-1heptene	19549-87-2	
6	5.629	C_8H_{16}	5-methylhept-1-ene	13151-04-7	3.6554
		$C_{10}H_{20}$	3,7-dimethyloct-1-ene	4984/1/4	
			annulene	629-20-9	
7	6.601	C_8H_8	benzocyclobutene	694-87-1	13.6182
			styrene	100-42-5	
8	8.277	C_9H_{10}	2-phenyl-1-propene	98-83-9	0.1321
9	8.717	$C_{10}H_{22}$	3-ethyl-3-methyl heptane	17302-01-1	0.1538
10	8.793	$C_{11}H_{24}$	2,6-dimethylnonane	17302-28-2	0.1761
11	9.148	$C_{10}H_{16}$	(3R)-(+)-Isosylvestren	1461-27-4	0.6663
12	9.91	$C_{13}H_{28}O$	11-methyl-1-dodecanol	85763-57-1	0.3317
13	9.978	$C_{13}H_{28}O$	11-methyl-1-dodecanol	85763-57-1	0.2899
14	13.352	$C_{13}H_{28}O$	11-methyl-1-dodecanol	85763-57-1	0.1570
15	13.474	$C_{13}H_{28}O$	11-methyl-1-dodecanol	85763-57-1	0.0933
16	13.596	$C_{13}H_{28}O$	11-methyl-1-dodecanol	85763-57-1	0.1712

Table A2. GC–MS analysis results of the rubber pyrolysis volatiles.

No.	Peaks	Formula	Compound	CAS Number	Yield/%
1	2.249	C_5H_{12}	2-methylbutane	78-78-4	7.2044
2	2.439	$C_6H_{14}O$	2-methyl-1-pentanol	105-30-6	0.5324

Table A2. *Cont.*

No.	Peaks	Formula	Compound	CAS Number	Yield/%
3	2.544	C_6H_{12}	1-hexene	592-41-6	3.9098
		C_6H_{12}	methylcyclopentane	96-37-7	
		$C_6H_{13}Cl$	2-chlorohexane	638-28-8	
4	2.958	C_6H_{10}	bipropenyl	592-46-1	0.5624
5	3.054	C_6H_6	benzene	71-43-2	0.6028
6	3.304	C_7H_{14}	1-heptene	592-76-7	1.8165
7	3.406	C_7H_{16}	heptane	142-82-5	0.4222
8	3.599	C_7H_{12}	2,4-dimethyl-1,3-pentadiene	1000-86-8	0.1327
9	3.999	C_7H_{10}	1-methyl-1,4-cyclohexadiene	4313-57-9	0.5747
10	4.197	$C_{10}H_{16}O$	3-hydroxy-2-methyl-6-methylene-1,7-octadiene	22459-10-5	0.6420
11	4.376	$C_9H_{12}O$	1-phenyl-2-propanol	698-87-3	1.8206
12	4.662	C_8H_{16}	2-methyl-1-heptene	15870-10-7	0.4028
13	4.747	C_8H_{16}	oct-1-ene	111-66-0	0.6065
		$C_8H_{18}O$	octan-1-ol	111-87-5	
14	4.9	C_8H_{18}	octane	111-65-9	0.4613
15	5.065	$C_8H_{14}O$	oct-2-yn-1-ol	20739-58-6	0.1743
16	5.635	C_9H_{18}	2,4-dimethyl-1-heptene	19549-87-2	6.3153
17	6.037	C_8H_{10}	ethylbenzene	100-41-4	0.2325
18	6.21	$C_{12}H_{16}O$	2-phenyl-hex-5-en-3-ol	77383-06-3	0.5773
19	6.601	$C_{12}H_{14}O_2$	2,2-dimethyl-5-phenyloxolan-3-one	63678-00-2	3.2998
20	6.752	C_9H_{20}	nonane	111-84-2	0.3576
21	7.903	$C_{21}H_{26}O_2$	benzoic acid-(2,4-di-tert-butyl-phenyl ester)	39000-49-2	0.1512
22	8.439	$C_{10}H_{20}$	1-decene	872-05-9	0.5524
23	8.595	$C_{10}H_{22}$	decane	124-18-5	0.2374
24	8.722	$C_{10}H_{22}$	3,3,5-trimethylheptane	7154-80-5	0.1590
25	8.819	$C_{16}H_{34}$	hexadecane	544-76-3	0.4068
26	9.068	$C_8H_{18}O$	2-ethylhexan-1-ol	104-76-7	0.4132
27	9.261	$C_{10}H_{12}O$	2-phenylbut-3-en-1-ol	6052-63-7	0.1071
28	9.91	$C_{13}H_{28}O$	11-methyl-1-dodecanol	85763-57-1	0.4746
29	10.163	$C_{11}H_{22}$	1-undecene	821-95-4	0.3116
30	10.302	$C_{11}H_{24}$	undecane	1120-21-4	0.1645
31	10.69	$C_{15}H_{32}O$	3,7,11-trimethyldodecan-1-ol	6750-34-1	0.1266
32	10.798	$C_{20}H_{40}O$	phytol	150-86-7	0.0440
33	11.064	$C_{16}H_{26}O_3$	2-dodecen-1-ylsuccinic anhydride	19780-11-1	0.0765
		$C_{10}H_{20}O$	cyclohexanemethanol, 2,4,6-trimethyl-	13702-56-2	
34	11.172	$C_{13}H_{18}O$	ether,isopropyl 2-benzyl-2-propenyl	900152-79-5	0.1764
35	11.645	$C_{12}H_{24}$	5-undecene,2-methyl-,(Z)-	74630-63-0	0.0857
36	11.753	$C_{12}H_{24}$	1-dodecene	112-41-4	0.1798
37	11.878	$C_{17}H_{37}N$	1-aminoheptadecane	4200-95-7	0.0804
38	13.355	$C_{18}H_{38}O$	2-hexyldodecan-1-ol	110225-00-8	0.5847
		$C_{13}H_{28}O$	11-methyl-1-dodecanol	85763-57-1	

Table A3. GC–MS analysis results of the leather pyrolysis volatiles.

No.	Peaks	Formula	Compound	CAS Number	Yield/%
1	2.246	$C_8H_{16}O$	1-prop-2-enoxypentane	23186-70-1	7.4626
2	2.439	$C_5H_{10}O$	3-penten-2-ol	1569-50-2	0.7402
3	2.53	C_6H_{12}	2-methyl-1-pentene	763-29-1	2.7042
			1-hexene	592-41-6	
4	2.952	C_6H_{10}	bipropenyl	592-46-1	0.4749
5	3.052	C_6H_6	benzene	71-43-2	0.5936
6	3.307	$C_7H_{16}O$	(s)-3,4-dimethylpentanol	900143-83-9	0.3582

Table A3. *Cont.*

No.	Peaks	Formula	Compound	CAS Number	Yield/%
7	3.4	C_7H_{16}	heptane	142-82-5	0.5957
8	4.361	$C_9H_{12}O$	1-phenyl-2-propanol	698-87-3	2.6530
9	4.722/4.88/5.039	C_8H_{16}	trans-1-butyl-2-methylcyclopropane	38851-70-6	2.5389
			cis-1-butyl-2-methylcyclopropane	38851-69-3	
			trans-2-octene	13389-42-9	
			trans-4-octene	14850-23-8	
		$C_8H_{17}Cl$	4-chlorooctane	999-07-5	
			3-chlorooctane	1117-79-9	
10	5.618	C_9H_{18}	2,4-dimethyl-1-heptene	19549-87-2	9.8874
11	6.017	C_8H_{10}	ethylbenzene	100-41-4	1.1988
12	6.59	C_8H_8	styrene	100-42-5	4.8862
13	7.894	C_9H_{12}	3-ethyltoluene	620-14-4	0.2492
14	8.215	C_9H_{12}	1-ethyl-4-methylbenzene	622-96-8	0.1529
			1-ethyl-2-methylbenzene	611-14-3	
			3-ethyltoluene	620-14-4	
15	8.269	C_9H_{10}	2-phenyl-1-propene	98-83-9	0.2948
16	8.427	$C_{14}H_{28}$	(e)-tetradec-3-ene	41446-68-8	0.1934
17	8.586	$C_{10}H_{22}$	decane	124-18-5	0.1247
18	8.708	$C_{10}H_{22}$	3-ethyl-3-methylheptane	17302-01-1	0.1877
19	8.807	$C_{20}H_{17}NO_2$	6-methyl-dodecane	6044-71-9	0.4697
20	9.054	$C_8H_{18}O$	2-ethylhexan-1-ol	104-76-7	0.8314
21	9.244	C_9H_{10}	indane	496-11-7	0.2027
22	9.902/9.973/13.349	$C_{13}H_{28}O$	11-methyl-1-dodecanol	85763-57-1	2.2638

Table A4. GC–MS analysis results of the textiles pyrolysis volatiles.

No.	Peaks	Formula	Compound	CAS Number	Yield/%
1	2.238	$C_4H_{11}NO$	O-(2-methylpropyl)hydroxylamine	5618-62-2	6.9797
2	2.45	$C_6H_{14}O$	2,3-dimethylbutyl alcohol	19550-30-2	0.4687
3	2.533	C_6H_{12}	2-methyl-1-pentene	763-29-1	3.7191
			1-hexene	592-41-6	
4	3.043	C_6H_6	benzene	71-43-2	3.4949
5	4.191	C_8H_{16}	2,3-dimethylhex-1-ene	16746-86-4	0.3236
			2,5-dimethyl-2-hexene	3404-78-2	
			(E)-2,3-dimethylhex-3-ene	7145-23-5	
6	4.364	$C_9H_{12}O$	1-phenyl-2-propanol	698-87-3	2.9873
7	5.133	C_9H_{18}	cis-1,1,3,4-tetramethylcyclopentane	53907-60-1	0.2179
8	5.272	C_9H_{20}	2,4-dimethyl-heptane	2213-23-2	0.0875
9	5.459	$C_{10}H_{18}$	isocitronellene	85006-04-8	0.3957
10	5.629	C_8H_{16}	5-methylhept-1-ene	13151-04-7	16.0668
11	5.972	C_9H_{18}	1,3,5-trimethyl-cyclohexane	1839-63-0	0.3468
12	6.026	C_8H_{10}	ethylbenzene	100-41-4	0.3153
13	6.599	C_8H_8	styrene	100-42-5	11.6357
14	6.973	$C_{10}H_{18}$	2,5-dimethyl-1,trans-6-octadien	68702-25-0	0.1709
15	7.208	C_9H_{12}	cumene	98-82-8	0.0322
16	7.616	C_9H_{10}	prop-2-enylbenzene	300-57-2	0.0838
17	7.767	$C_{13}H_{18}O_2$	phenylacetic acid isoamyl ester	102-19-2	0.0935
18	7.92	C_7H_6O	benzaldehyde	100-52-7	0.1585
19	8.277	C_9H_{10}	2-phenyl-1-propene	98-83-9	0.9701
20	8.43	$C_{16}H_{32}$	hexadec-3-ene	34303-81-6	0.3858
21	8.717/8.787	$C_{14}H_{30}$	dodecane,4,6-dimethyl	61141-72-8	0.6796
		$C_{11}H_{24}$	2,6-dimethylnonane	17302-28-2	
22	9.907/9.981	$C_{13}H_{28}O$	11-methyl-1-dodecanol	85763-57-1	2.3873
23	10.236	$C_8H_8O_2$	methyl benzoate	93-58-3	0.0960
24	10.684/10.792	$C_{15}H_{32}O$	3,7,11-trimethyldodecan-1-ol	6750-34-1	0.1598
25	10.894	$C_9H_8O_2$	vinyl benzoate	769-78-8	0.1427
26	11.064	$C_{10}H_{20}O$	dihydoisocyclogeraniol	13702-56-2	0.1177
27	11.45	$C_9H_{10}O_2$	ethyl benzoate	93-89-0	0.1083
28	13.355/13.474/13.590	$C_{13}H_{28}O$	11-methyl-1-dodecanol	85763-57-1	1.5021

Table A5. GC–MS analysis results of the foam pyrolysis volatiles.

No.	Peaks	Formula	Compound	CAS Number	Yield/%
1	2.226	$C_6H_{12}O_2$	1-isopropoxy-propan-2-one	42781-12-4	6.6008
2	2.399	$C_3H_6N_2O_2$	cycloserine	68-41-7	0.6897
3	2.884	$C_6H_{14}O$	1-propan-2-yloxypropane	627-08-7	1.3509
4	3.188	$C_6H_{12}O$	2,2,3,3-tetramethyloxirane	5076-20-0	1.9050
5	3.502	$C_{17}H_{34}O_2$	2-(tetradecoxymethyl)oxirane	38954-75-5	0.4383
6	3.689	$C_6H_{12}O_2$	2,2,4-Trimethyl-1,3-dioxolane	1193-11-9	1.2745
7	3.908	$C_6H_{10}O_2$	4-methylpentane-2,3-dione	7493-58-5	0.3843
8	4.067	$C_{11}H_{22}O_2$	2-ethylhexyl glycidyl ether	2461-15-6	0.7434
9	4.361	C_7H_8	toluene	108-88-3	1.3903
10	4.79	$C_8H_{18}O_2$	1-(1-propoxyethoxy)propane	105-82-8	2.6692
11	5.135	$C_6H_{12}O_2$	1-isopropoxy-propan-2-one	42781-12-4	5.3007
12	5.532	$C_6H_{12}O_2$	2,2,4-trimethyl-1,3-dioxolane	1193-11-9	0.1558
13	5.62	$C_{10}H_{20}O$	decanal	112-31-2	0.2558
14	5.728	$C_6H_{13}NO$	hexanamide	628-02-4	0.3094
15	6.023	C_8H_{10}	ethylbenzene	100-41-4	0.4235
16	6.599	C_8H_8	annulene styrene	629-20-9 100-42-5	11.9324
17	7.078	$C_7H_{16}O$	4-methylhexan-3-ol	615-29-2	0.0498
18	7.738	$C_7H_{16}O$	2-propan-2-yloxybutane	18641-81-1	0.3678
19	7.869	$C_8H_{18}O$	4-methyl-3-heptanol	14979-39-6	0.2974
20	8.274	C_9H_{10}	2-phenyl-1-propene	98-83-9	0.4722
21	8.337	$C_6H_{12}O_2$	5-methoxypentan-2-one	17429-04-8	1.5136
22	9.071	$C_8H_{18}O$	6-methyl-1-heptanol	1653-40-3	0.3426
23	9.13	$C_8H_{17}Cl$	3-chlorooctane	1117-79-9	0.3620

References

1. Nourreddine, M. Recycling of auto shredder residue. *J. Hazard. Mater.* **2007**, *139*, 481–490. [CrossRef] [PubMed]
2. Fiore, S.; Ruffino, B.; Zanetti, M.C. Automobile Shredder Residues in Italy: Characterization and valorization opportunities. *Waste Manag.* **2012**, *32*, 1548–1559. [CrossRef] [PubMed]
3. Cossu, R.; Fiore, S.; Lai, T.; Luciano, A.; Mancini, G.; Ruffino, B.; Viotti, P.; Zanetti, M.C. Review of Italian experience on automotive shredder residue characterization and management. *Waste Manag.* **2014**, *34*, 1752–1762. [CrossRef] [PubMed]
4. Ruffino, B.; Fiore, S.; Zanetti, M.C. Strategies for the enhancement of automobile shredder residues (ASRs) recycling: Results and cost assessment. *Waste Manag.* **2014**, *34*, 148–155. [CrossRef]
5. Ahmed, N.; Wenzel, H.; Hansen, J.B. Characterization of Shredder Residues generated and deposited in Denmark. *Waste Manag.* **2014**, *34*, 1279–1288. [CrossRef]
6. Cossu, R.; Lai, T. Automotive shredder residue (ASR) management: An overview. *Waste Manag.* **2015**, *45*, 143–151. [CrossRef]
7. Morselli, L.; Santini, A.; Passarini, F.; Vassura, I. Automotive shredder residue (ASR) characterization for a valuable management. *Waste Manag.* **2010**, *30*, 2228–2234. [CrossRef]
8. Passarini, F.; Ciacci, L.; Santini, A.; Vassura, I.; Morselli, L. Auto shredder residue LCA: Implications of ASR composition evolution. *J. Clean. Prod.* **2012**, *23*, 28–36. [CrossRef]
9. Mancini, G.; Viotti, P.; Luciano, A.; Fino, D. On the ASR and ASR thermal residues characterization of full scale treatment plant. *Waste Manag.* **2014**, *34*, 448–457. [CrossRef]
10. Vermeulen, I.; Van Caneghem, J.; Block, C.; Baeyens, J.; Vandecasteele, C. Automotive shredder residue (ASR): Reviewing its production from end-of-life vehicles (ELVs) and its recycling, energy or chemicals' valorisation. *J. Hazard. Mater.* **2011**, *190*, 8–27. [CrossRef]
11. Roy, C.; Chaala, A. Vacuum pyrolysis of automobile shredder residues. *Resour. Conserv. Recycl.* **2001**, *32*, 1–27. [CrossRef]
12. Zolezzi, M.; Nicolella, C.; Ferrara, S.; Iacobucci, C.; Rovatti, M. Conventional and fast pyrolysis of automobile shredder residues (ASR). *Waste Manag.* **2004**, *24*, 691–699. [CrossRef]

13. Santini, A.; Passarini, F.; Vassura, I.; Serrano, D.; Dufour, J.; Morselli, L. Auto shredder residue recycling: Mechanical separation and pyrolysis. *Waste Manag.* **2012**, *32*, 852–858. [CrossRef] [PubMed]
14. Harder, M.K.; Forton, O.T. A critical review of developments in the pyrolysis of automotive shredder residue. *J. Anal. Appl. Pyrolysis* **2007**, *79*, 387–394. [CrossRef]
15. Ni, F.J.; Chen, M. Research on ASR in China and its energy recycling with pyrolysis method. *J. Mater. Cycles Waste Manag.* **2015**, *17*, 107–117. [CrossRef]
16. Haydary, J.; Susa, D.; Gelinger, V.; Čacho, F. Pyrolysis of automobile shredder residue in a laboratory scale screw type reactor. *J. Environ. Chem. Eng.* **2016**, *4*, 965–972. [CrossRef]
17. Mayyas, M.; Pahlevani, F.; Handoko, W.; Sahajwalla, V. Preliminary investigation on the thermal conversion of automotive shredder residue into value-added products: Graphitic carbon and nano-ceramics. *Waste Management* **2016**, *50*, 173–183. [CrossRef]
18. Anzano, M.; Collina, E.; Piccinelli, E.; Lasagni, M. Lab-scale pyrolysis of the Automotive Shredder Residue light fraction and characterization of tar and solid products. *Waste Manag.* **2017**, *64*, 263–271. [CrossRef]
19. Notarnicola, M.; Cornacchia, G.; De Gisi, S.; Di Canio, F.; Freda, C.; Garzone, P.; Martino, M.; Valerio, V.; Villone, A. Pyrolysis of automotive shredder residue in a bench scale rotary kiln. *Waste Manag.* **2017**, *65*, 92–103. [CrossRef]
20. Evangelopoulos, P.; Sophonrat, N.; Jilvero, H.; Yang, W. Investigation on the low-temperature pyrolysis of automotive shredder residue (ASR) for energy recovery and metal recycling. *Waste Manag.* **2018**, *76*, 507–515. [CrossRef]
21. Yang, B.; Chen, M. Influence of Interactions among Polymeric Components of Automobile Shredder Residue on the Pyrolysis Temperature and Characterization of Pyrolytic Products. *Polymers* **2020**, *12*, 1682. [CrossRef] [PubMed]
22. He, M.; Hu, Z.; Xiao, B.; Li, J.; Guo, X.; Luo, S.; Yang, F.; Feng, Y.; Yang, G.; Liu, S. Hydrogen-rich gas from catalytic steam gasification of municipal solid waste (MSW): Influence of catalyst and temperature on yield and product composition. *Int. J. Hydrog. Energy* **2009**, *34*, 195–203. [CrossRef]
23. He, M.; Xiao, B.; Liu, S.; Hu, Z.; Guo, X.; Luo, S.; Yang, F. Syngas production from pyrolysis of municipal solid waste (MSW) with dolomite as downstream catalysts. *J. Anal. Appl. Pyrolysis* **2010**, *87*, 181–187. [CrossRef]
24. Blanco, P.H.; Wu, C.; Onwudili, J.A.; Williams, P.T. Characterization and evaluation of Ni/SiO2 catalysts for hydrogen production and tar reduction from catalytic steam pyrolysis-reforming of refuse derived fuel. *Appl. Catal. B Environ.* **2013**, *134–135*, 238–250. [CrossRef]
25. He, M.; Xiao, B.; Liu, S.; Guo, X.; Luo, S.; Xu, Z.; Feng, Y.; Hu, Z. Hydrogen-rich gas from catalytic steam gasification of municipal solid waste (MSW): Influence of steam to MSW ratios and weight hourly space velocity on gas production and composition. *Int. J. Hydrog. Energy* **2009**, *34*, 2174–2183. [CrossRef]
26. Acomb, J.C.; Wu, C.; Williams, P.T. Control of steam input to the pyrolysis-gasification of waste plastics for improved production of hydrogen or carbon nanotubes. *Appl. Catal. B Environ.* **2014**, *147*, 571–584. [CrossRef]
27. Donaj, P.; Blasiak, W.; Yang, W.; Forsgren, C. Conversion of microwave pyrolysed ASR's char using high temperature agents. *J. Hazard. Mater.* **2011**, *185*, 472–481. [CrossRef]
28. Lin, K.-S.; Chowdhury, S.; Wang, Z.-P. Catalytic gasification of automotive shredder residues with hydrogen generation. *J. Power Sources* **2010**, *195*, 6016–6023. [CrossRef]
29. Kai, X.; Li, R.; Yang, T.; Shen, S.; Ji, Q.; Zhang, T. Study on the co-pyrolysis of rice straw and high density polyethylene blends using TG-FTIR-MS. *Energy Convers. Manag.* **2017**, *146*, 20–33. [CrossRef]
30. Wu, J.; Chen, T.; Luo, X.; Han, D.; Wang, Z.; Wu, J. TG/FTIR analysis on co-pyrolysis behavior of PE, PVC and PS. *Waste Manag.* **2014**, *34*, 676–682. [CrossRef]
31. Zhang, J.; Chen, T.; Wu, J.; Wu, J. TG-MS analysis and kinetic study for thermal decomposition of six representative components of municipal solid waste under steam atmosphere. *Waste Manag.* **2015**, *43*, 152–161. [CrossRef] [PubMed]
32. Singh, S.; Wu, C.; Williams, P.T. Pyrolysis of waste materials using TGA-MS and TGA-FTIR as complementary characterisation techniques. *J. Anal. Appl. Pyrolysis* **2012**, *94*, 99–107. [CrossRef]
33. Guo, Q.J.; Zhang, X.; Li, C.; Liu, X.M.; Li, J.H. TG-MS study of the thermo-oxidative behavior of plastic automobile shredder residues. *J. Hazard. Mater.* **2012**, *209*, 443–448. [CrossRef] [PubMed]
34. Mayyas, M.; Pahlevani, F.; Bucknall, M.; Maroufi, S.; You, Y.; Liu, Z.; Sahajwalla, V. Thermocatalytic Conversion of Automotive Shredder Waste and Formation of Nanocarbons as a Process Byproduct. *Acs Sustain. Chem. Eng.* **2017**, *5*, 5440–5448. [CrossRef]

35. Gao, Z.; Nakada, M.; Amasaki, I. A consideration of errors and accuracy in the isoconversional methods. *Thermochim. Acta* **2001**, *369*, 137–142. [CrossRef]
36. Guan, Y.; Luo, S.; Liu, S.; Xiao, B.; Cai, L. Steam catalytic gasification of municipal solid waste for producing tar-free fuel gas. *Int. J. Hydrog. Energy* **2009**, *34*, 9341–9346. [CrossRef]
37. Arregi, A.; Amutio, M.; Lopez, G.; Artetxe, M.; Alvarez, J.; Bilbao, J.; Olazar, M. Hydrogen-rich gas production by continuous pyrolysis and in-line catalytic reforming of pine wood waste and HDPE mixtures. *Energy Convers. Manag.* **2017**, *136*, 192–201. [CrossRef]
38. Duman, G.; Yanik, J. Two-step steam pyrolysis of biomass for hydrogen production. *Int. J. Hydrog. Energy* **2017**, *42*, 17000–17008. [CrossRef]
39. Al-Salem, S.M.; Antelava, A.; Constantinou, A.; Manos, G.; Dutta, A. A review on thermal and catalytic pyrolysis of plastic solid waste (PSW). *J. Environ. Manag.* **2017**, *197*, 177–198. [CrossRef]
40. Almeida, D.; Marques, M.d.F. Thermal and Catalytic Pyrolysis of Plastic Waste. *Polímeros* **2016**, *26*, 44–51. [CrossRef]